PNAS

Supplementary Information for

Follistatin regulates the specification of the apical cochlea responsible for low-frequency hearing in mammals

Hei Yeun Koo[1,2], Min-A Kim[3], Hyehyun Min[1], Jae Yeon Hwang[4], Meenakshi Prajapati-DiNubila[5], Kwan Soo Kim[1,2], Martin M. Matzuk[6], Juw Won Park[4], Angelika Doetzlhofer[5], Un-Kyung Kim[3], Jinwoong Bok[1,2,7]*

[1]Department of Anatomy, Yonsei University College of Medicine, Seoul 03722, Korea.
[2]Brain Korea 21 Project for Medical Science, Yonsei University College of Medicine, Seoul 03722, Korea.
[3]Department of Biology, Kyungpook National University, Daegu 41566, Korea.
[4]Department of Computer Science and Engineering, University of Louisville, Louisville, Kentucky 40292, United States.
[5]The Solomon H. Snyder Department of Neuroscience, Johns Hopkins University, School of Medicine, Baltimore, Maryland 21205, United States.
[6]Department of Pathology & Immunology and Center for Drug Discovery, Baylor College of Medicine, Houston, Texas 77030, United States.
[7]Department of Otorhinolaryngology, Yonsei University College of Medicine, Seoul 03722, Korea.

* Corresponding author: Jinwoong Bok
Email: bokj@yuhs.ac,
ORCID: 0000-0003-1958-1872

This PDF file includes:

Materials and Methods

Mice strains and generation of crosses

Fst$^{-/-}$ and *Inhba*$^{-/-}$ mice were purchased from the Jackson Laboratory (JAX, 002788 and 002990, respectively; Bar Harbor, ME, USA) (1, 2). Inner ear-specific *Fst* cKO mice were generated by crossing *Fst*$^{lox/lox}$ mice (3) with *Pax2-Cre* transgenic mice (4). Inner ear-specific *Smo* gain-of-function mutants were generated by crossing *SmoM2* mice (*Gt(ROSA)26Sor*$^{tm1(Smo/EYFP)Amc}$/J, JAX 005130) with *Pax2-Cre* mice. Inner ear-specific *Smo* loss-of-function mutants were generated by crossing *Smo*$^{lox/lox}$ mice (*Smo*^{tm2Amc}/J, JAX 004526) with *Emx2*^{Cre} mice (RBRC02272, RIKEN, Tokyo, Japan). For fate-mapping of *Msx1*-positive cells, *Msx1*$^{CreERT2/+}$ mice (B6.129S2(Cg)-*Msx1*$^{tm2.1(cre/ERT2)Bero}$/J, JAX 027850) were crossed with *R26-tdTomato* mice (B6.Cg-*Gt(ROSA)26Sor*$^{tm14(CAG-tdTomato)Hze}$/J, JAX 007914). *Msx1*$^{CreERT2/+}$; *R26-tdTomato* mice were further crossed with *Fst*$^{+/-}$ mice to generate *Msx1*$^{CreERT2/+}$; *R26-tdTomato*; *Fst*$^{-/-}$ mice. *R26-FST* mice overexpressing human *FST* upon doxycycline administration were generated by crossing *R26-M2rtTA* mice with *FST* transgenic mice, as previously described (5). Mice were mated, and the morning of vaginal plug formation was counted as E0.5. All animal protocols were approved by the Institutional Animal Care and Use Committee at Yonsei University College of Medicine, Seoul, Korea, and at Johns Hopkins University School of Medicine, Baltimore, United States, in accordance with NIH guidelines.

Paint-fill injections to visualize the inner ear

To visualize the gross morphology of the inner ear, paint-fill injections were performed as previously described (6). Briefly, E15.5 embryos were harvested, fixed in Bodian's fixative, dehydrated in ethanol, and cleared in methyl salicylate. Correction fluid in methyl salicylate (1:800) was injected inside the lumen of the inner ear by inserting a micropipette on the lateral surface of the inner ear ampulla.

In situ hybridization and measurement of signal intensities

Whole or hemi-sectioned heads of embryos from E11.75 to E16.5 were fixed in 4% paraformaldehyde, dehydrated in 30% sucrose, and embedded in Tissue-Tek optimum cutting temperature compound. Inner ear tissues were sectioned at 12-μm thickness using a cryostat (HM525, Thermo Fisher Scientific, Waltham, MA, USA) and subjected to *in situ* hybridization as previously described (6). Antisense RNA probes for apical markers (*Fst*, *Msx1*, *Slitrk3*, *Efnb2*), basal markers (*A2m* and *Inhba*), and SHH readouts (*Gli1* and *Ptch1*) were prepared as previously described (7-9). Micrographs of gene expression patterns were acquired using a DM2500 optical microscope (Leica, Wetzlar, Germany). All *in situ* hybridization images shown are representative of at least three different samples in two or more independent experiments.

Measurement of *in situ* hybridization signal intensities was performed as previously described (10). Briefly, images of all cochlear sections were collected and numbered from the base to the apex. *In situ* hybridization signal intensities were measured using Multi Gauge software (FUJIFILM, Tokyo, Japan) by positioning a rectangle on the cochlear epithelial region exhibiting *in situ* hybridization signals. The signal intensity within the rectangle was defined as the quantum level (Q), and the signal intensity within a same-sized rectangle positioned in a nearby epithelial or mesenchymal region without *in situ* hybridization signal was defined as the background level (B). The intensity of the *in situ* hybridization signal (QB) in each cochlear section was calculated by subtracting B from Q. Cochlear sections that were obliquely sectioned because of the coil structure were excluded from analysis. For each gene, the lowest QB value among all sections

with a positive signal was defined as the “threshold QB,” and the relative signal intensity of each section was then calculated as follows:

Equation 1:

$$\%\ \text{intensity of a section} = \frac{(\text{QB value of a section}) - (\text{threshold QB value})}{(\text{highest QB value among all sections}) - (\text{threshold QB value})}$$

The *in situ* hybridization signal with the highest QB value among all cochlear sections from a wild-type mouse was designated as 100% intensity, and the signal matching the threshold QB value was designated as 0% intensity. The percent intensities of each section from wild-type and mutant cochleae (y-axis) were then plotted against their respective section number from the base to the apex (x-axis).

Phalloidin staining

Inner ear tissues were fixed in 4% paraformaldehyde overnight, and the cochlear epithelium was isolated by removing the lateral wall, Reissner’s membrane, and the spiral ganglia. The dissected cochlear tissues were stained with phalloidin labeled with Alexa Fluor 568 (1:250, A12380, Thermo Fisher Scientific). Immunolabeled cochlear tissues were mounted with ProLong™ Gold Antifade Mountant (P36930, Thermo Fisher Scientific), and images were acquired using a confocal microscope (LSM 780, Zeiss, Oberkochen, Germany).

Fate-mapping of *Msx1*-lineage cells and measurement of fluorescent intensity

To genetically label *Msx1*-expressing cells in the presence or absence of *Fst*, *Msx1*$^{CreERT2/+}$; *R26-tdTomato*; *Fst*$^{+/-}$ mice were crossed with *R26-tdTomato*; *Fst*$^{-/-}$ mice. Tamoxifen (3 mg/40 g, T5648, MilliporeSigma, Burlington, MA, USA) was intraperitoneally injected into pregnant female mice at E11.5, and embryos were harvested at E18.5. Cochlear tissues were isolated with the cochlear lateral wall retained to preserve *Msx1*-expressing cells, and the cochlear tissues were stained with phalloidin labeled with Alexa Fluor 488 (1:250, A12379, Thermo Fisher Scientific) and 4′,6-diamidino-2-phenylindole dihydrochloride (DAPI) (1:1000, D1306, Thermo Fisher Scientific). Images were taken using a confocal microscope in tile scan mode (LSM 980, Zeiss). TdTomato and DAPI fluorescence intensities were determined using ZEN software (Zeiss) by measuring fluorescent intensities in 100 μm × 100 μm square boxes drawn and numbered along the entire length of each cochlea from base to apex. Normalized tdTomato fluorescence intensities were divided by the corresponding DAPI intensities and plotted on the y-axis according to box number from the base to the apex (x-axis).

EdU staining and counting

Pregnant female mice were injected intraperitoneally with EdU (Thermo Fisher Scientific) at 10 mg/g body weight at three time points (10:00 AM, 12:00 PM, and 2:00 PM) on E12.5. Then, embryos were harvested at E18.5. Hair cells were labeled with anti-MYO7A antibody (1:200, 25-6790, Proteus BioSciences, Waltham, MA, USA), and EdU-positive cells were labeled using a Click-iT EdU Cell Proliferation Kit for Imaging with Alexa Fluor 488 dye (C10337, Thermo Fisher Scientific). Images of whole cochleae were acquired using a confocal microscope (LSM 700, Zeiss). Each cochlear duct was divided into five regions: 10%–18%, 28%–36%, 46%–54%, 64%–72%, and 82%–90%. From the basal end, these represented the base, mid-base, mid, mid-apex,

and apex of the cochlea, respectively. The numbers of EdU-positive cells were counted in the lateral non-sensory compartment located equidistant to the three rows of outer hair cells, and the percentages of EdU-positive hair cells were determined by counting EdU-positive cells among the MYO7A-positive cells in each cochlear region. The cochlear length was determined by measuring along the outermost outer hair cells using ImageJ (NIH) (11).

TUNEL staining

TUNEL staining was performed as previously described (7) on inner ear sections prepared for *in situ* hybridization using the ApopTag Plus Peroxidase *In Situ* Apoptosis Kit (S7101, MilliporeSigma). The sections were fixed in 1% paraformaldehyde, permeabilized in a 2:1 pre-cooled ethanol to acetic acid solution, quenched in 3% H_2O_2, and incubated with terminal deoxynucleotidyl transferase for 1 hour. The sections were then conjugated with anti-digoxigenin peroxidase, stained with peroxidase substrate (3,3′-diaminobenzidine), and counterstained with methyl green (M8884, MilliporeSigma). The slides were mounted using Synthetic Mountant (6769007, Thermo Scientific). Micrographs were acquired using a Leica DM2500 optical microscope.

Scanning electron microscopy and measurements

Cochlear samples from 4-week-old and P15 mice were prepared for scanning electron microscopy (SEM) as previously described (12). Images were acquired using a cold field-emission scanning electron microscope (JSM-7001F; JEOL, Tokyo, Japan). For measurements of stereocilia length, SEM images were taken from the side to visualize the tallest stereocilia. For measurements of stereocilia angle and numbers, SEM images were taken from above to visualize the V-shaped hair bundle morphology. SEM images obtained from whole cochleae were combined using ImageJ (NIH) (11). The cochlear regions were divided into five regions covering 10%–18%, 28%–36%, 46%–54%, 64%–72%, and 82%–90% from the basal end. The basal (0%–10%) and apical (90%–100%) tip regions were excluded from measurement because the stereocilia in these regions often exhibit irregular morphologies that prevent reliable measurements. The stereocilia length for each hair cell was determined by measuring and averaging the lengths of the three tallest stereocilia using ImageJ (NIH). The stereocilia angles were measured using ImageJ (NIH), and the number of stereocilia on each hair cell were manually counted. All measurements were taken from at least 30 hair cells in each cochlear region from at least three different control and mutant mice. The values were plotted as box plots using Prism 7.0 software (GraphPad Software, San Diego, CA, USA). In the box plots, individual dots represent individual values, the box indicates the 25%–75% interquartile range, the horizontal lines indicate the median, the whiskers indicate the 5% and 95% values, and the points outside the whiskers represent outliers.

RNA-Seq sample preparation and data analysis

For sequencing library construction, cochleae were dissected from 4-week-old control ($Fst^{lox/lox}$) and *Fst* cKO mutant mice and divided into three regions (base, middle, and apex) along the tonotopic axis. Each cochlear region from each genotype was pooled together and RNA was extracted. The RNA was divided into three technical replicates and prepared for sequencing using a TruSeq RNA Sample Prep Kit v2 (Illumina, San Diego, CA, USA). Libraries were quantified and subjected to a 101-cycle paired-end sequence run using a TruSeq SBS Kit v3 on a HiSeq 4000 sequencer (Illumina). Sequencing data were generated while controlling the system

via the HiSeq Control Software v3.3. Base calling was performed with Real Time Analysis v2.5.2 (Illumina). The binary base calls (BCLs) were converted into FASTQ files using the bcl2fastq package v2.16.0.10 (Illumina). Sequencing reads as FASTQ files with three replicates of each sample group were aligned to the *Mus musculus* genome (assembly GRCm38) with STAR aligner v2.5.2b. Read counts and FPKM values were calculated based on the mouse GRCm38 Ensembl Release 82 gene annotation. Cuffdiff v2.2.1 was used to search differentially expressed genes (DEGs), setting pairwise comparisons for all sample groups at once. Cuffdiff output data were then used for downstream analysis in R v3.5.0. PCA was performed based on FPKM values using the prcomp and ggplot2 packages in R. Heatmaps were generated using hierarchical clustering via the heatmap.2 package in R. Functional annotation clustering analysis was conducted using the Database for Annotation, Visualization, and Integrated Discovery (DAVID) as previously published (13). Biological annotations with an enrichment score > 1.5, a $P < 0.05$, and a false discovery rate (FDR) < 5% were considered biologically interesting. Possible upstream regulators were analyzed using Ingenuity Pathway Analysis (Qiagen, Hilden, Germany). Genes in the UP, UP-1, DOWN, and DOWN-1 groups were used for analysis, and a cutoff value of <0.01 was used to adjust the significant candidate genes.

Genes differentially expressed along the tonotopic axis

Significant DEGs along the tonotopic axis of mature cochleae were determined from genes with an average FPKM ≥ 1.0 in at least one of the six sample groups (base, middle, and apex for control or *Fst* cKO). There were 14,994 (32.2%) genes out of 46,597 Ensembl annotated genes in this category. Among these, 612 genes in control ($Fst^{lox/lox}$) mice showed at least a 1.5-fold increase in FPKM from base to apex, allowing a 5% variable against directionality. These were classified as the UP group. Likewise, 730 genes showed at least a 1.5-fold decrease from base to apex and were categorized as the DOWN group. Among the 612 genes in the UP group, 128 genes met the following conditions in *Fst* cKO mice compared with controls mice and were categorized as the UP-1 group: 1) FPKM value at the apex reduced by more than 25%, 2) percent increase from base to apex reduced by more than 25% (equation 2), or 3) percent increase from middle to apex reduced more than 50% (equation 3).

Equation 2:

$$\frac{\text{Control Apex}-\text{Control Base}}{\text{Control Base}} \times 0.75 \geq \frac{\text{cKO Apex}-\text{cKO Base}}{\text{cKO Base}}$$

Equation 3:

$$\frac{\text{Control Apex}-\text{Control Mid}}{\text{Control Mid}} \times 0.5 \geq \frac{\text{cKO Apex}-\text{cKO Mid}}{\text{cKO Mid}}$$

Among the 730 genes in the DOWN group, 269 genes met the following conditions in *Fst* cKO mice compared with control mice and were categorized as the DOWN-1 group: 1) FPKM value at the apex increased by more than 25%, 2) percent decrease from base to apex increased by more than 25% (equation 4), or 3) percent decrease from middle to apex increased by more than 50% (equation 5).

Equation 4:

$$\frac{\text{Control Base}-\text{Control Apex}}{\text{Con Base}} \times 0.75 \geq \frac{\text{cKO Base}-\text{cKO Apex}}{\text{cKO Base}}$$

Equation 5:

$$\frac{\text{Control Mid}-\text{Control Apex}}{\text{Con Apex}} \times 0.5 \geq \frac{\text{cKO Mid}-\text{cKO Apex}}{\text{cKO Apex}}.$$

Auditory brainstem response

ABR thresholds were measured as previously described (12). Subdermal needles (electrodes) were positioned at the vertex and ventrolateral to the right and left ear of anesthetized mice. Calibrated click stimuli (10 μs duration) or tone burst stimuli (5 ms duration) at 4, 6, 8, 10, 12, 18, 24, and 30 kHz were produced using the SigGenRZ software package and an RZ6 digital signal processor (Tucker-Davis Technologies, Alachua, FL, USA). These were delivered to the ear canal through a Multi-Field 1 (MF1) magnetic speaker (Tucker-Davis Technologies). The stimulus intensity was increased from 10 to 95 dB sound pressure level (SPL) in 5 dB SPL increments. The ABR signals were fed into a low-impedance Medusa Biological Amplifier System (RA4LI, Tucker-Davis Technologies), which then was used to deliver the signal to the RZ6 digital signal processing hardware. The recorded signals were filtered using a 0.5–1 kHz band-pass filter, and the ABR waveforms in response to 512 tone bursts were averaged. The ABR thresholds for each frequency were determined using the BioSigRZ software package (Tucker-Davis Technologies). Wave I amplitudes were determined at two specific frequencies (6 and 18 kHz) by calculating P1-N1 peak amplitudes (in nV) as I/O functions with stimulus levels increased from 30 to 90 dB SPL in 10 dB SPL increments.

Distortion product otoacoustic emissions

DPOAE thresholds were measured as previously described (12). Primary stimulus tones were produced using an RZ6 digital signal processor and the SigGenRZ software package (Tucker-Davis Technologies). These were delivered through a custom probe containing an ER-10B+ microphone (Etymotic Research, Elk Grove Village, IL, USA) with Multi-Field 1 speakers (Tucker-Davis Technologies) positioned in the ear canal. The primary tones were set at a frequency ratio (f_2/f_1) of 1.2 with target frequencies at 6, 8, 10, 12, 16, 18, 24, and 30 kHz. The f_1 and f_2 intensities were set at equal levels (L1 = L2) and increased from 20 to 80 dB SPL in 5 dB SPL increments. The resultant sounds in response to the primary tones were received by the ER-10B+ microphone in the custom probe and recorded using the RZ6 digital signal processor (Tucker-Davis Technologies). The I/O functions for the DPOAEs were determined at two specific frequencies ($2f_1$-f_2 = 6 and 18 kHz). At each primary tone for each intensity of the I/O functions, the fast Fourier transform was performed using the BioSigRZ software package (Tucker-Davis Technologies) to determine the average spectra of the two primaries, the $2f_1$-f_2 distortion products, and the noise floors.

Statistical analysis

Statistical comparisons were made via two-way analysis of variance (ANOVA) with Bonferroni corrections for multiple comparisons for the EdU graph, stereociliary morphology (length, angle, and number), ABRs, and DPOAEs. T-tests were used to compare cochlear length. Analyses were performed with Prism 7.0 software (GraphPad Software). All statistically analyzed data were graphed as means ± standard error. Statistical significance is indicated in the figures as n.s. (non-significant; $P > 0.05$), *$P < 0.05$, **$P < 0.01$, ***$P < 0.001$, and ****$P < 0.0001$.

Supplementary Figures

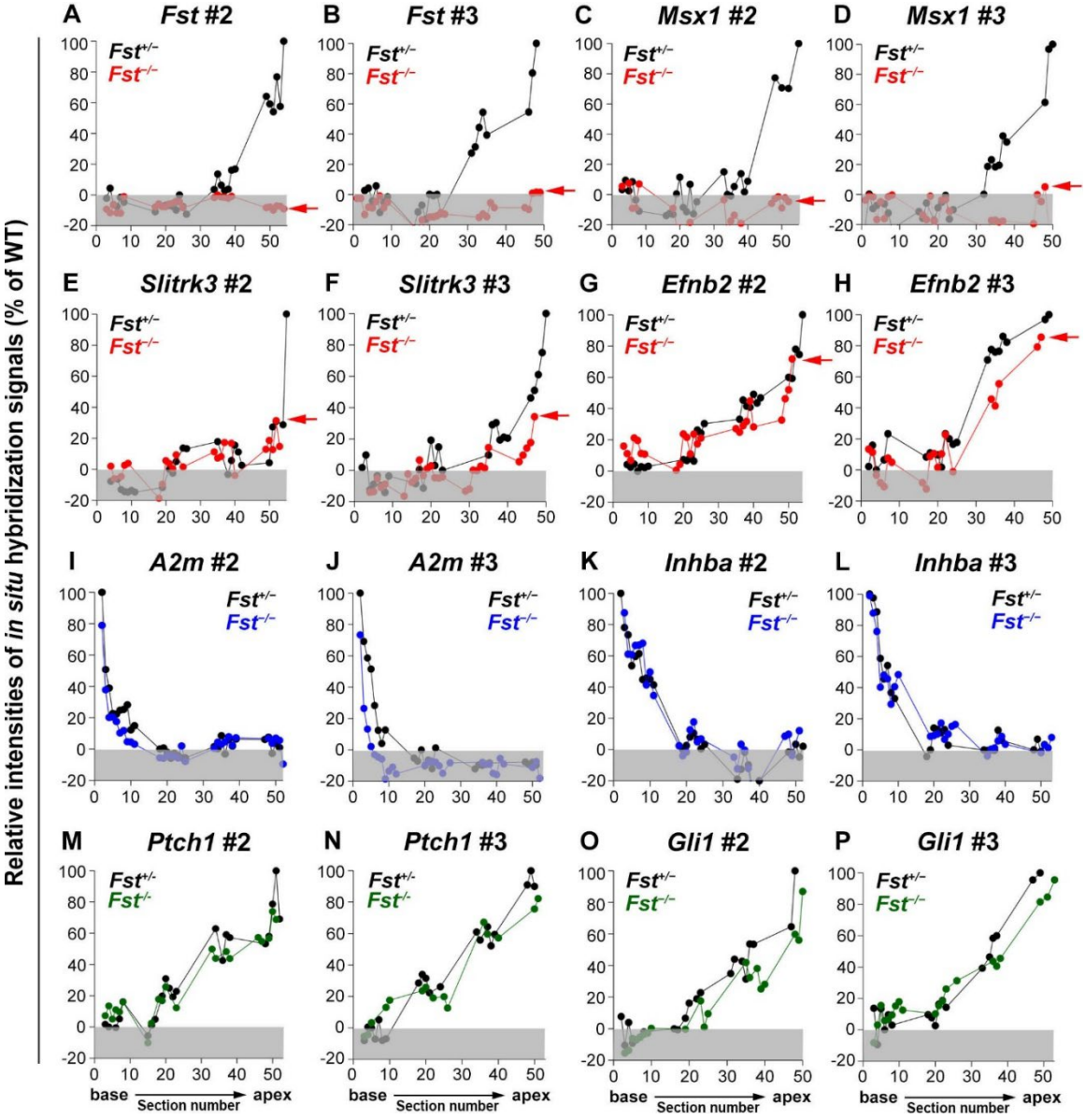

Fig. S1. Additional examples of *in situ* hybridization signal intensities along the cochlear duct. Relative signal intensities of apical markers such as *Fst, Msx1, Slitrk3,* and *Efnb2* (**A–H**), basal markers such as *A2m* and *Inhba* (**I–L**), and SHH target genes such as *Ptch1* and *Gli1* (**M–P**) along the cochlear duct of $Fst^{+/-}$ and $Fst^{-/-}$ embryos at E15.5.

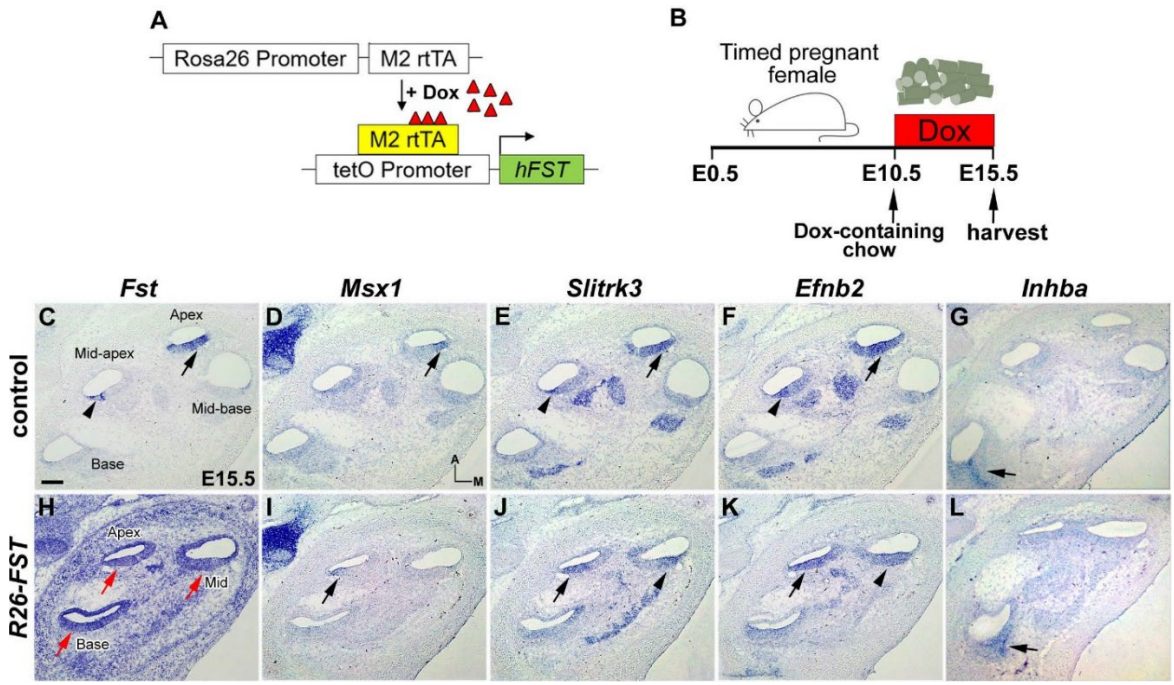

Fig. S2. Ectopic *FST* expression does not alter the expression patterns of regional cochlear markers. (**A–B**) Schematic of the inducible *FST* transgenic mouse model. In *R26-M2rtTA*; *tetO-human FST* double transgenic mice (*R26-FST*), *FST* was expressed under the control of the R26 promoter in the presence of doxycycline (Dox) (**A**). Doxycycline-containing chow was provided to pregnant female mice beginning at E10.5, and the embryos were harvested at E15.5 (**B**). (**C–L**) *In situ* hybridization of apical (*Fst*, *Msx1*, *Slitrk3*, and *Efnb2*) and basal (*Inhba*) markers in control and *R26-FST* embryos. Arrows and arrowheads indicate relatively strong and weak expression levels, respectively. Red arrows indicate up-regulation of expression. The scale bar in **C**, 100 μm, also applies to **D–L**.

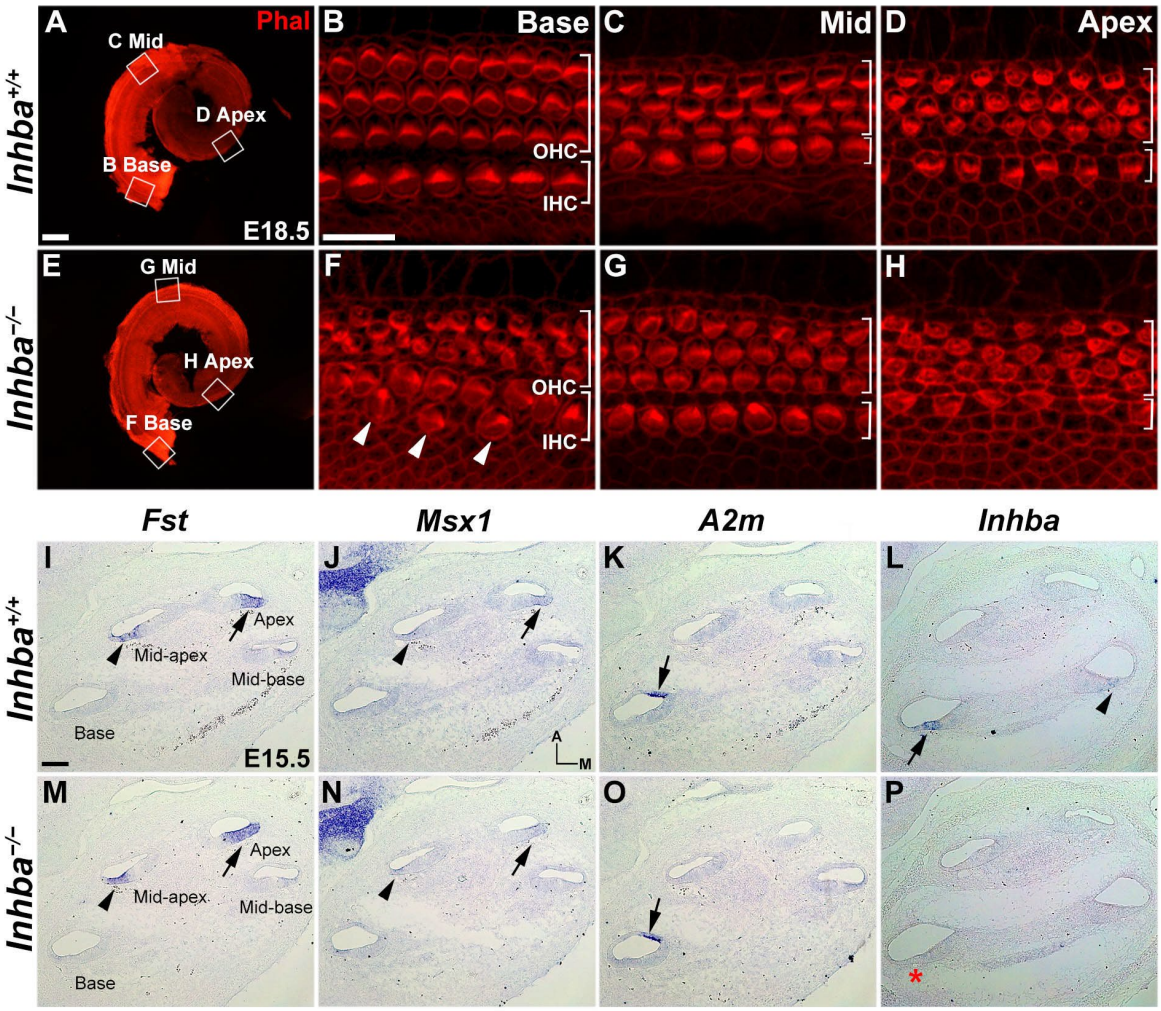

Fig. S3. Graded expression patterns of regional cochlear markers remain unchanged in *Inhba*$^{-/-}$ embryos. (**A–H**) Whole-mount phalloidin staining of cochlear sensory epithelia from *Inhba*$^{+/+}$ and *Inhba*$^{-/-}$ embryos at E18.5. Arrowheads indicate ectopic inner hair cells. (**I–P**) *In situ* hybridization for apical (*Fst* and *Msx1*) and basal (*A2m* and *Inhba*) markers. The scale bar in **A**, 200 μm, also applies to **E**. The scale bar in **B**, 10 μm, also applies to **C–D** and **F–H**. The scale bar in **I**, 100 μm, also applies to **J–P**.

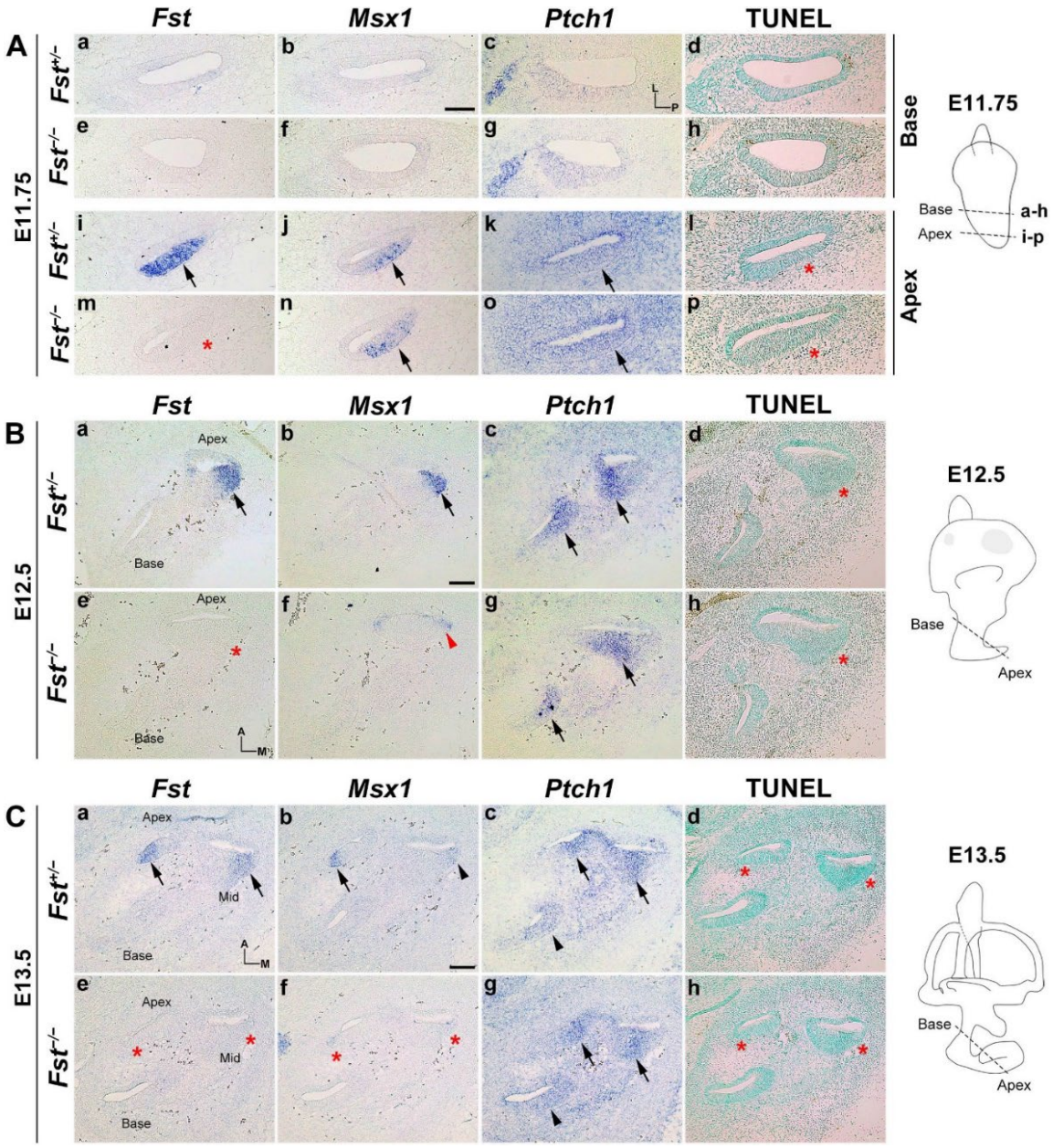

Fig. S4. Apical identity is gradually lost during cochlear development in *Fst*$^{-/-}$ embryos. *In situ* hybridization analysis of *Fst*, *Msx1*, and *Ptch1*, as well as TUNEL staining, in *Fst*$^{+/-}$ and *Fst*$^{-/-}$ embryos during early cochlear development at E11.75 (**A**), E12.5 (**B**), and E13.5 (**C**). Arrows and arrowheads indicate relatively strong and weak expression levels, respectively. Red asterisks and red arrowheads indicate absence or down-regulation of expression. The scale bars in **Ab** (100 μm), **Bb** (100 μm), and **Cb** (100 μm), apply to all the images in **A**, **B**, and **C**, respectively.

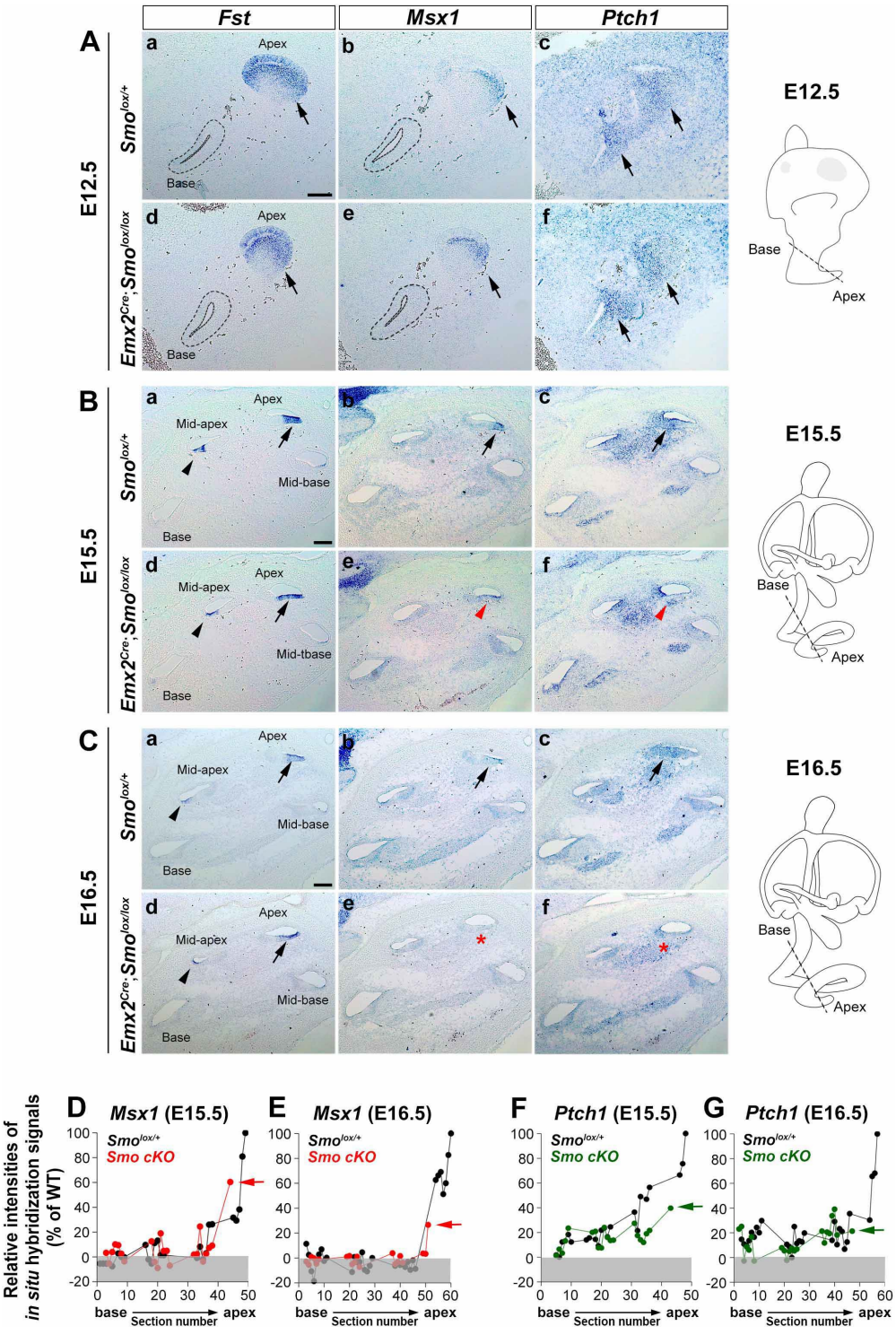

Fig. S5. Apical identity is gradually lost in the absence of sustained SHH signaling. *In situ* hybridization analysis of *Fst*, *Msx1*, and *Ptch1* in *Smo*$^{lox/+}$ and *Emx2*^{Cre}; *Smo*$^{lox/lox}$ embryos at E12.5 (**A**), E15.5 (**B**), and E16.5 (**C**). Arrows and arrowheads indicate relatively strong and weak expression levels, respectively. Red asterisks and red arrowheads indicate absence or down-regulation of expression, respectively. (**D–G**) Relative *in situ* hybridization signal intensities along the cochlear duct in Smo$^{lox/+}$ and *Emx2*^{Cre}; *Smo*$^{lox/lox}$ embryos. The scale bars in **Ab** (100 μm), **Bb** (100 μm), and **Cb** (100 μm) apply to all the images in **A**, **B**, and **C**, respectively.

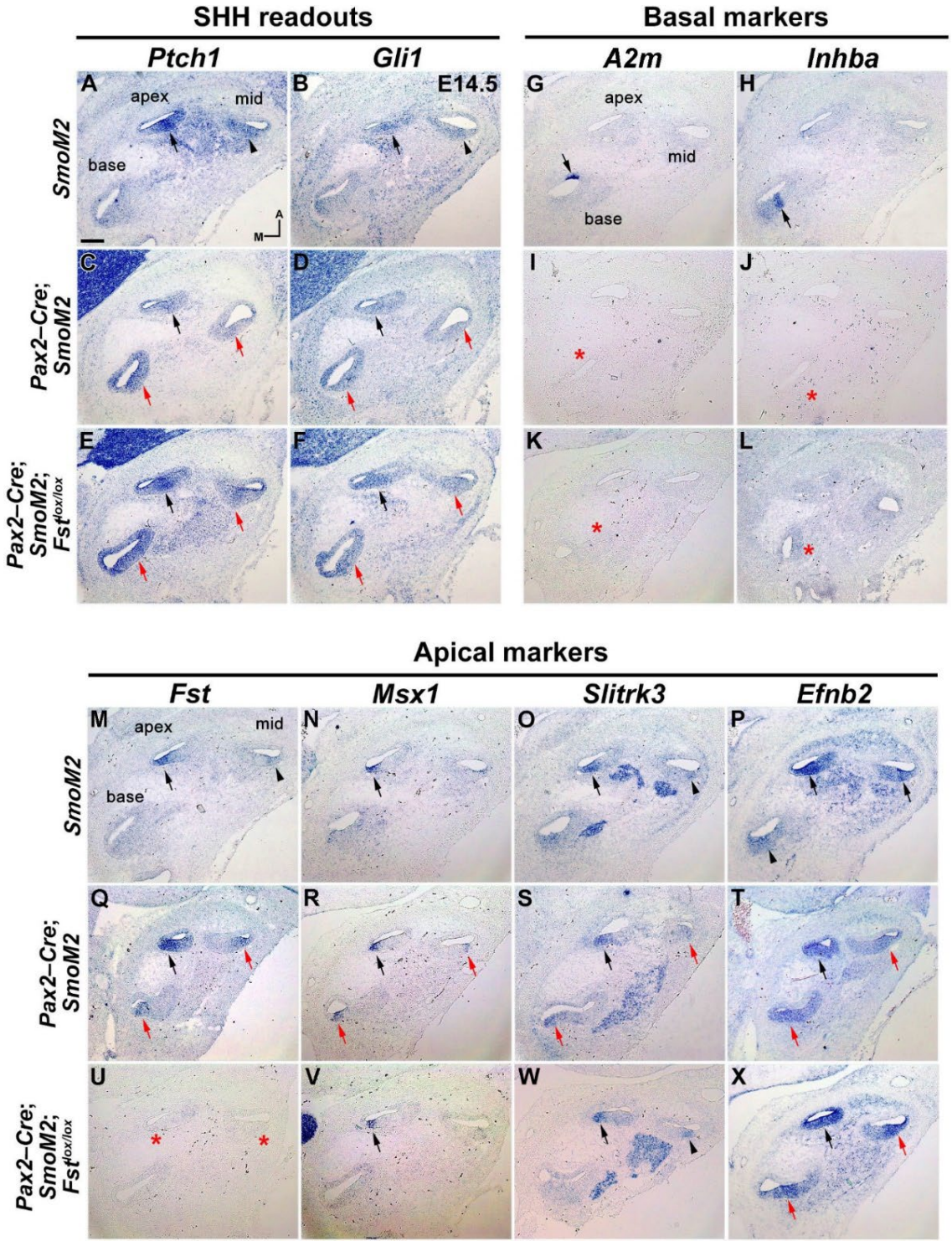

Fig. S6. FST is required for ectopic apical gene expression induced by strong SHH activity. *In situ* hybridization analysis of SHH readout genes (*Ptch1* and *Gli1*) (**A**–**F**), basal markers (*A2m* and *Inhba*) (**G**–**L**), and apical markers (*Fst, Msx1, Slitrk3,* and *Enfb2*) (**M**–**X**) in *Pax2-Cre*; *SmoM2* and *Pax2-Cre*; *SmoM2*; *Fst*$^{lox/lox}$ mutant cochleae at E14.5. Black arrows and arrowheads indicate relatively strong and weak expression levels, respectively. Red arrows indicate ectopic up-regulation, and red asterisks indicate absence of expression. The scale bar in **A**, 100 μm, also applies to **B**–**X**.

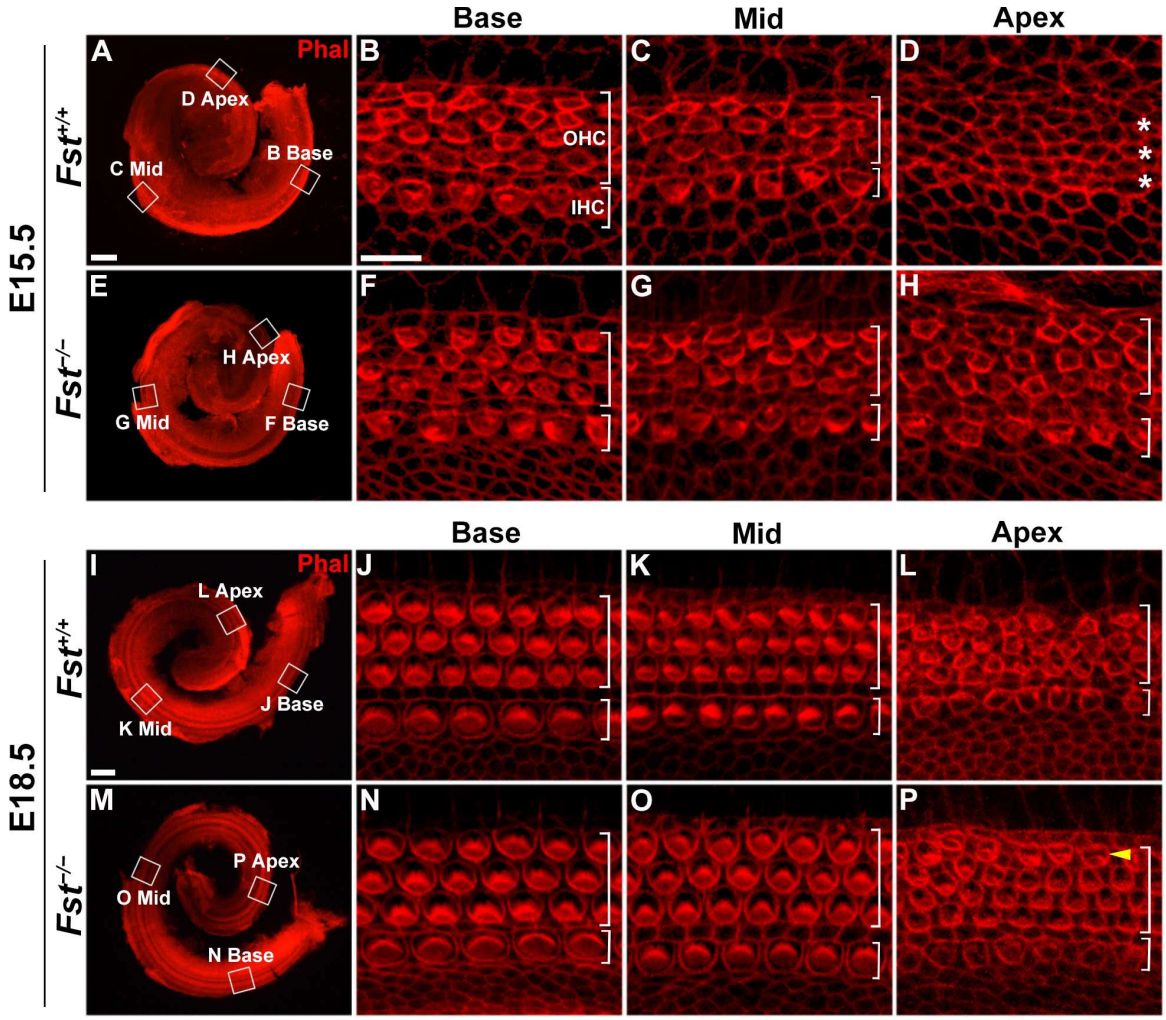

Fig. S7. Hair cells are differentiated slightly prematurely in *Fst*$^{-/-}$ embryos. Whole-mount phalloidin staining of cochleae from *Fst*$^{+/+}$ and *Fst*$^{-/-}$ embryos at E15.5 (**A–H**) and E18.5 (**I–P**). Brackets indicate one row of inner hair cells (IHC) and three rows of outer hair cells (OHC). The scale bar in **A**, 200 μm, also applies to **E, I,** and **M**. The scale bar in **B**, 10 μm, also applies to **C–D, F–H, J–L,** and **N–P**.

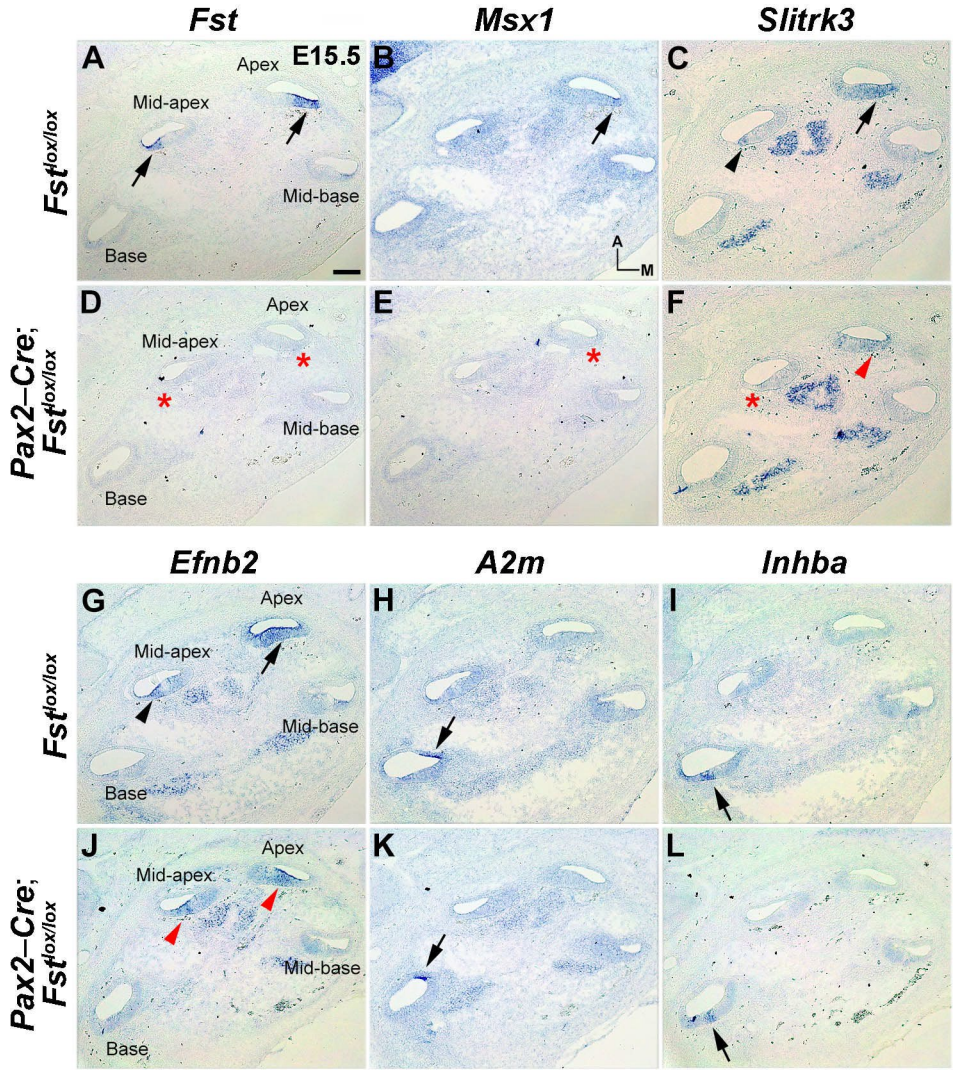

Fig. S8. Inner ear-specific *Fst* cKO recapitulates the expression patterns of regional markers in *Fst*$^{-/-}$ mice. *In situ* hybridization analysis of apical markers (*Fst*, *Msx1*, *Slitrk3*, *Efnb2*) and basal markers (*A2m*, *Inhba*) in *Pax2-Cre*; *Fst*$^{lox/lox}$ embryos at E15.5. Arrows and arrowheads indicate relatively strong and weak expression levels, respectively. Red asterisks and red arrowheads indicate absence or down-regulation of expression, respectively. The scale bar in **A**, 100 μm, applies to all panels.

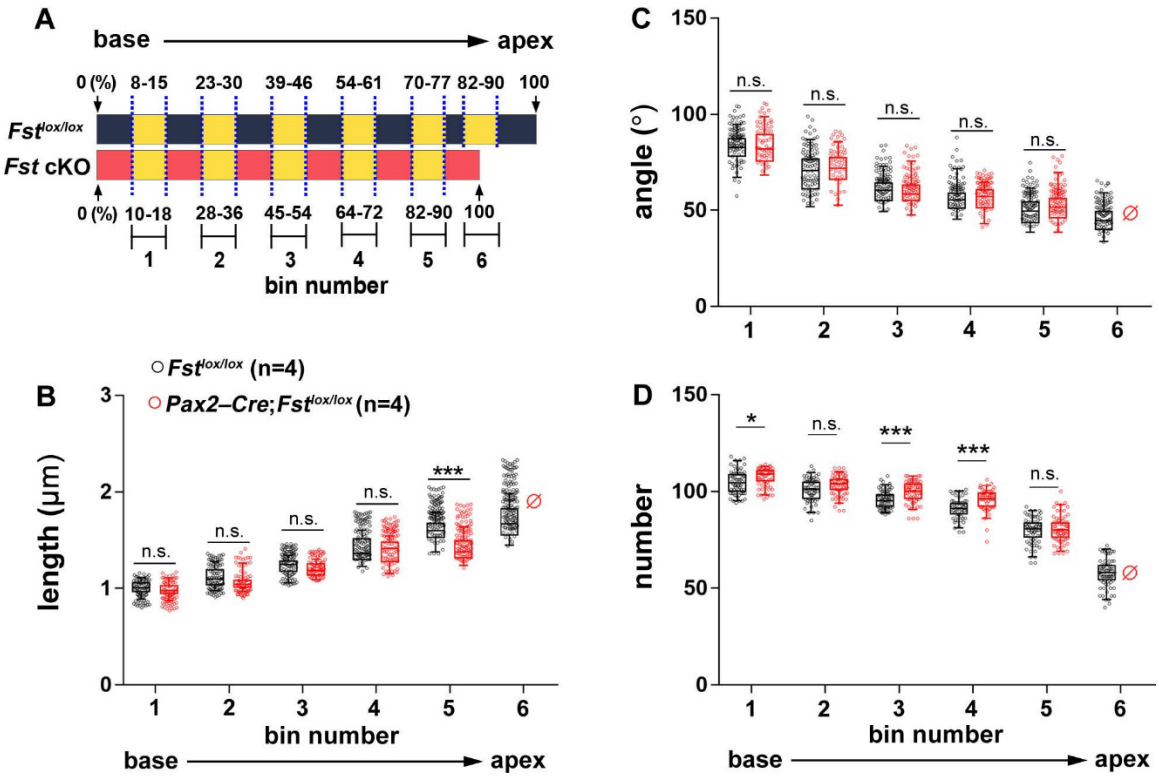

Fig. S9. Comparison of stereocilia morphologies equidistant from the basal end of control and *Fst* cKO cochleae. (**A**) Schematic showing the relative lengths of control and *Fst* cKO cochleae at 4 weeks. The numbers 1 to 6 indicate cochlear locations equidistant from the basal end of control and *Fst* cKO cochleae. Note that there is no bin #6 in *Fst* cKO mutants because of their shorter cochlear ducts. The apical region (82%–90%) of *Fst* cKO mutant cochleae corresponds to the mid-apical region (70%–77%) of controls. (**B-D**) Stereocilia length (**B**), angle (**C**), and number (**D**) were determined by measuring at least 30 outer hair cells per bin location from four different animals per genotype. Data are presented as box plots. Individual dots represent individual data values, boxes indicate the 25%–75% interquartile range, horizontal lines in the boxes indicate the median, whiskers indicate the 5% and 95% values, and the points outside the whiskers represent outliers. Statistical significance was determined via two-way ANOVA with Bonferroni corrections for multiple comparisons (n.s., non-significant, $*P < 0.05$, and $***P < 0.001$).

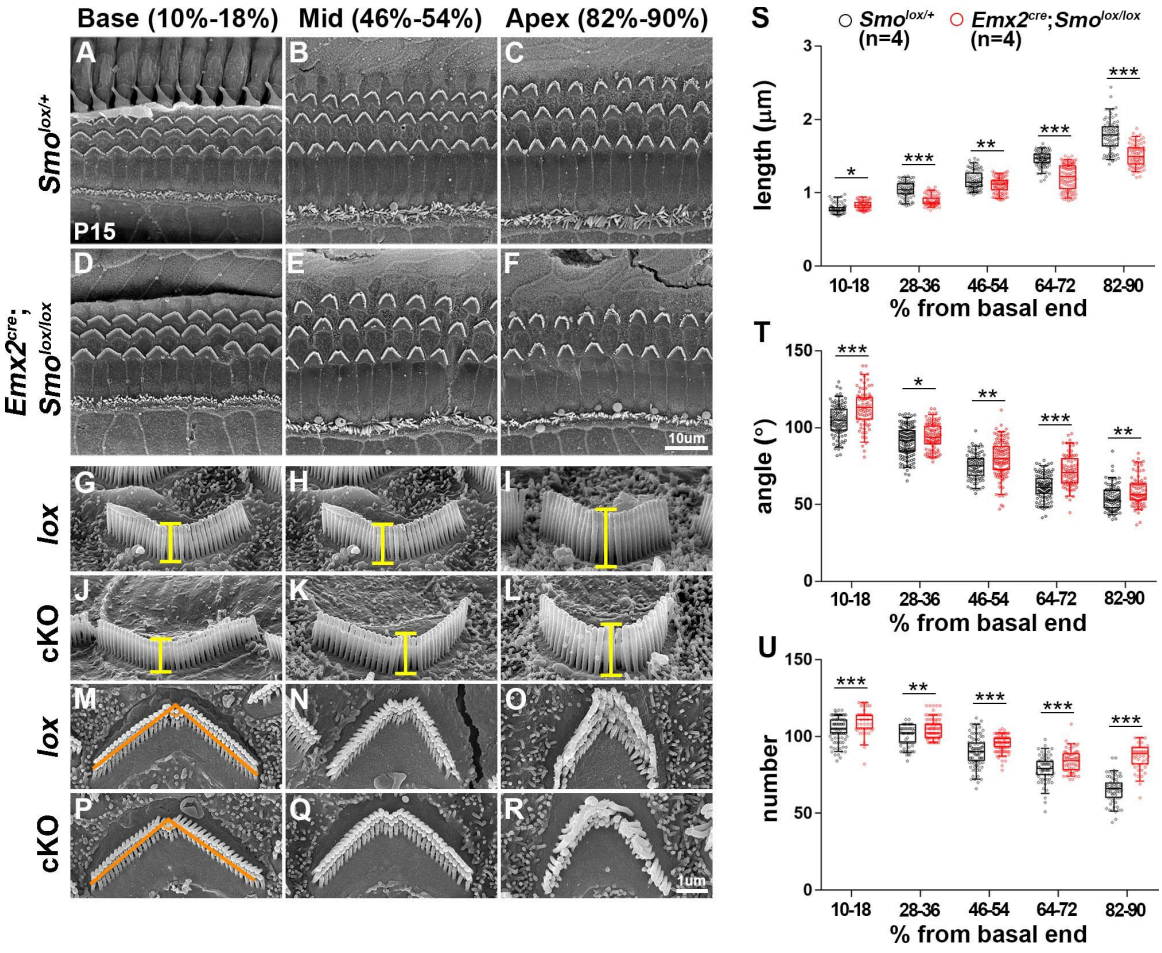

Fig. S10. Loss of apical characteristics in stereocilia bundle morphology in *Emx2*^{Cre}; *Smo*$^{lox/lox}$ mutants. (**A-R**) Scanning electron micrographs of the organ of Corti from control (lox) (*Smo*$^{lox/lox}$) and inner ear-specific *Smo* cKO (*Emx2*^{Cre}; *Smo*$^{lox/lox}$) mice. No obvious hair cell degeneration was observed except for the third row of outer hair cells at the apex in *Smo* cKO mice (**A-F**). The lengths of other hair cell stereocilia were measured at the vertex of the V-shaped hair bundles as viewed from the side (**G-L**). The angle of the V-shaped hair bundles and the number of stereocilia per hair cell were measured using a top-down view (**M-R**). (**S-U**) Quantification of stereocilia length, angle, and number along the tonotopic axis from five cochlear regions from the basal end, representing base (10%–18%), mid-base (28%–36%), mid (46%–54%), mid-apex (64%–72%), and apex (82%–90%). Data are displayed as box plots. Individual dots represent individual data values, the boxes indicate the 25%–75% interquartile range, the horizontal lines in the boxes indicate the median, the whiskers indicate the 5% and 95% values, and the points outside the whiskers represent outliers. Statistical comparisons were determined via two-way ANOVA with Bonferroni corrections for multiple comparisons (n.s., non-significant, $^{**}P < 0.01$, and $^{***}P < 0.001$).

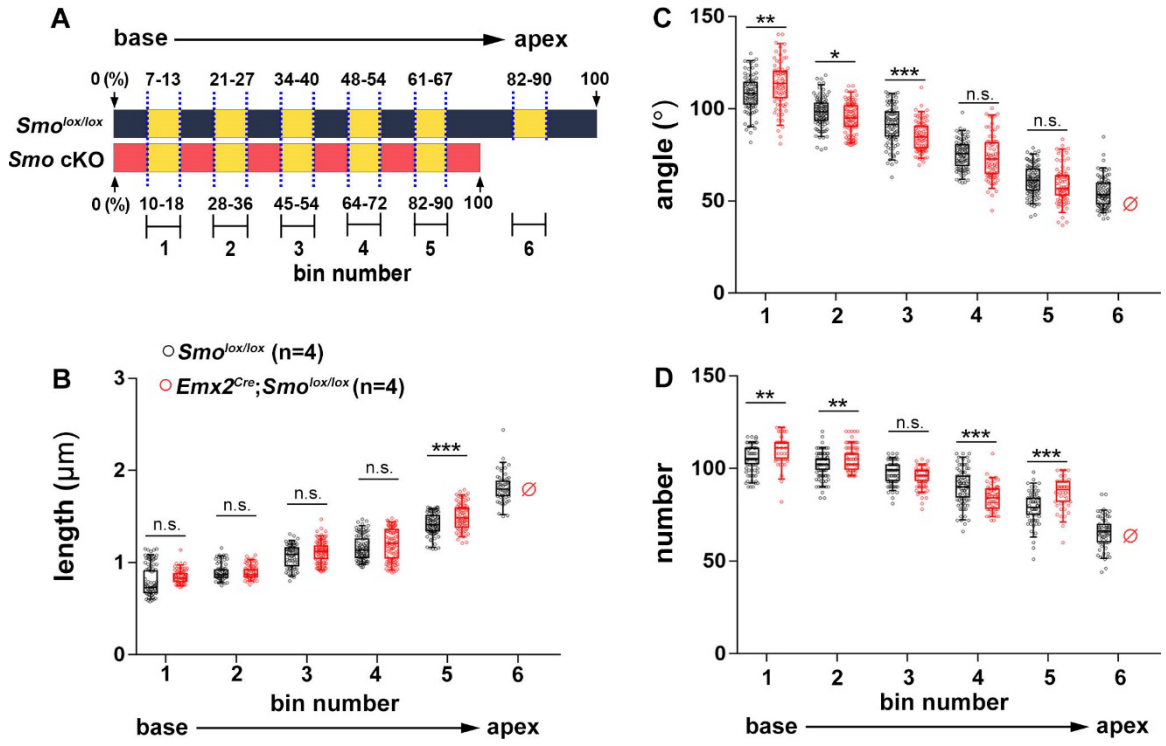

Fig. S11. Comparison of stereocilia morphologies equidistant from the basal end of control and *Smo* cKO cochleae. (**A**) Schematic showing the relative lengths of control and *Smo* cKO cochleae at P15. The numbers 1 to 6 indicate cochlear locations equidistant from the basal end of control and *Smo* cKO cochleae. Note that there is no bin #6 in *Smo* cKO mutants because of their shorter cochlear ducts. The apical region (82%–90%) of *Smo* cKO mutant cochleae corresponds to the mid-apical region (61%–67%) of controls. (**B-D**) Stereocilia length (**B**), angle (**C**), and number (**D**) were determined by measuring at least 30 outer hair cells per bin location from four different animals per genotype. Data are presented as box plots. Individual dots represent individual data values, boxes indicate the 25%–75% interquartile range, horizontal lines in the boxes indicate the median, whiskers indicate the 5% and 95% values, and the points outside the whiskers represent outliers. Statistical significance was determined via two-way ANOVA with Bonferroni corrections for multiple comparisons (n.s., non-significant, **P* < 0.05, and ****P* < 0.001).

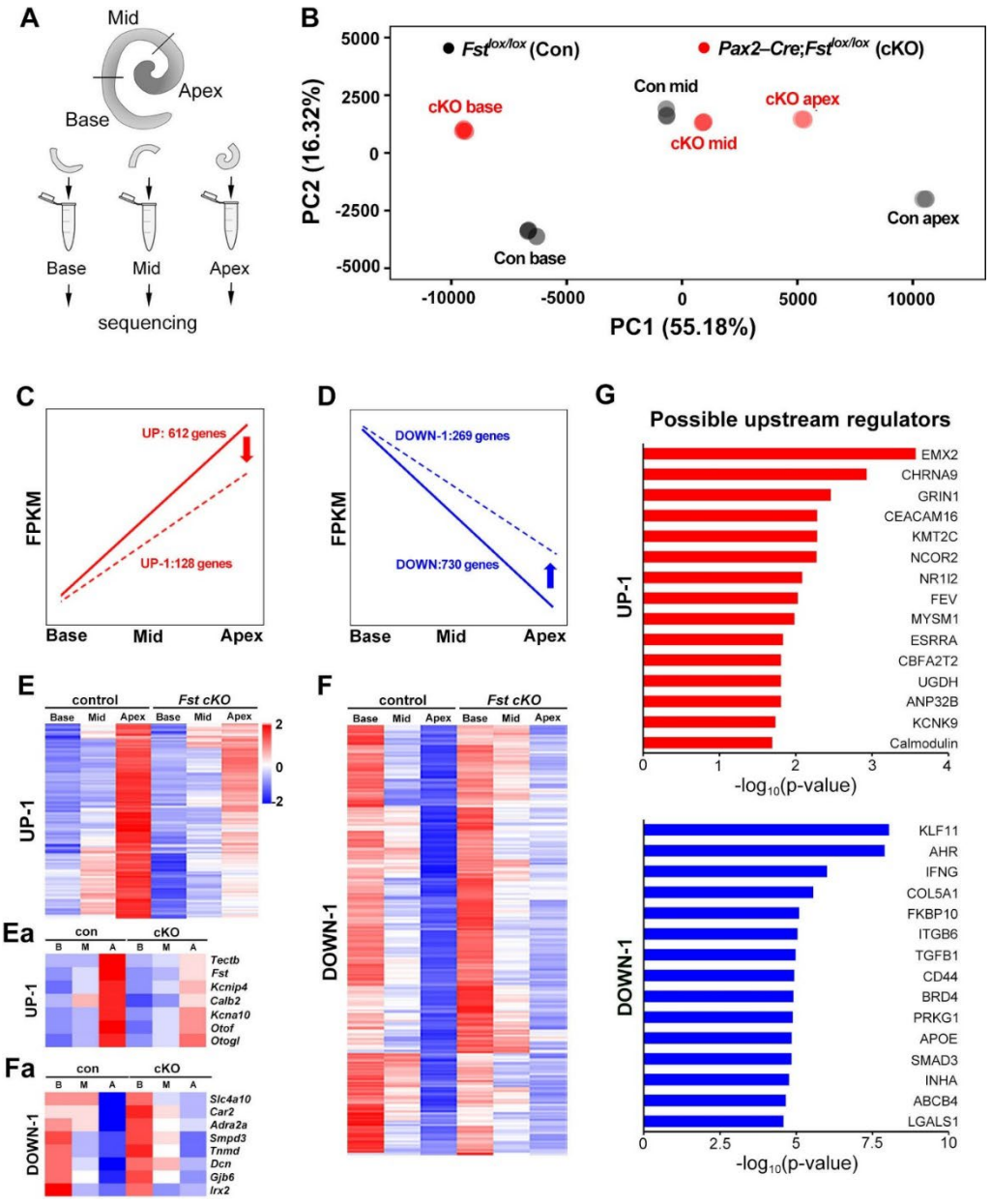

Fig. S12. Changes in gene expression in *Fst*-deficient cochleae. (**A**) A schematic detailing cochlear sample preparation for RNA-seq analysis of the base, middle, and apex of cochleae from 4-week-old control (con) (*Fst*$^{lox/lox}$) and inner ear-specific *Fst* cKO (*Pax2-Cre*; *Fst*$^{lox/lox}$) mice. (**B**) PCA using FPKM values obtained from RNA-seq of each cochlear region (base, mid, and apex) of each genotype (con and cKO). (**C–D**) Diagram depicting genes in the UP and DOWN groups with base-to-apex increasing or decreasing gradients with ≥ 1.5-fold change from control cochlea. The UP-1 or DOWN-1 group exhibited significant down-regulation or up-regulation at the apex or a less steep slope in *Fst* cKO cochleae (see Methods for details). (**E–F**) Heatmaps of the 128 genes in the UP-1 group and the 269 genes in the DOWN-1 group. (**Ea, Fa**) Examples of genes reported previously to be expressed in a graded pattern along the cochlear duct. (**G**) Possible upstream regulators of the UP-1 and DOWN-1 groups.

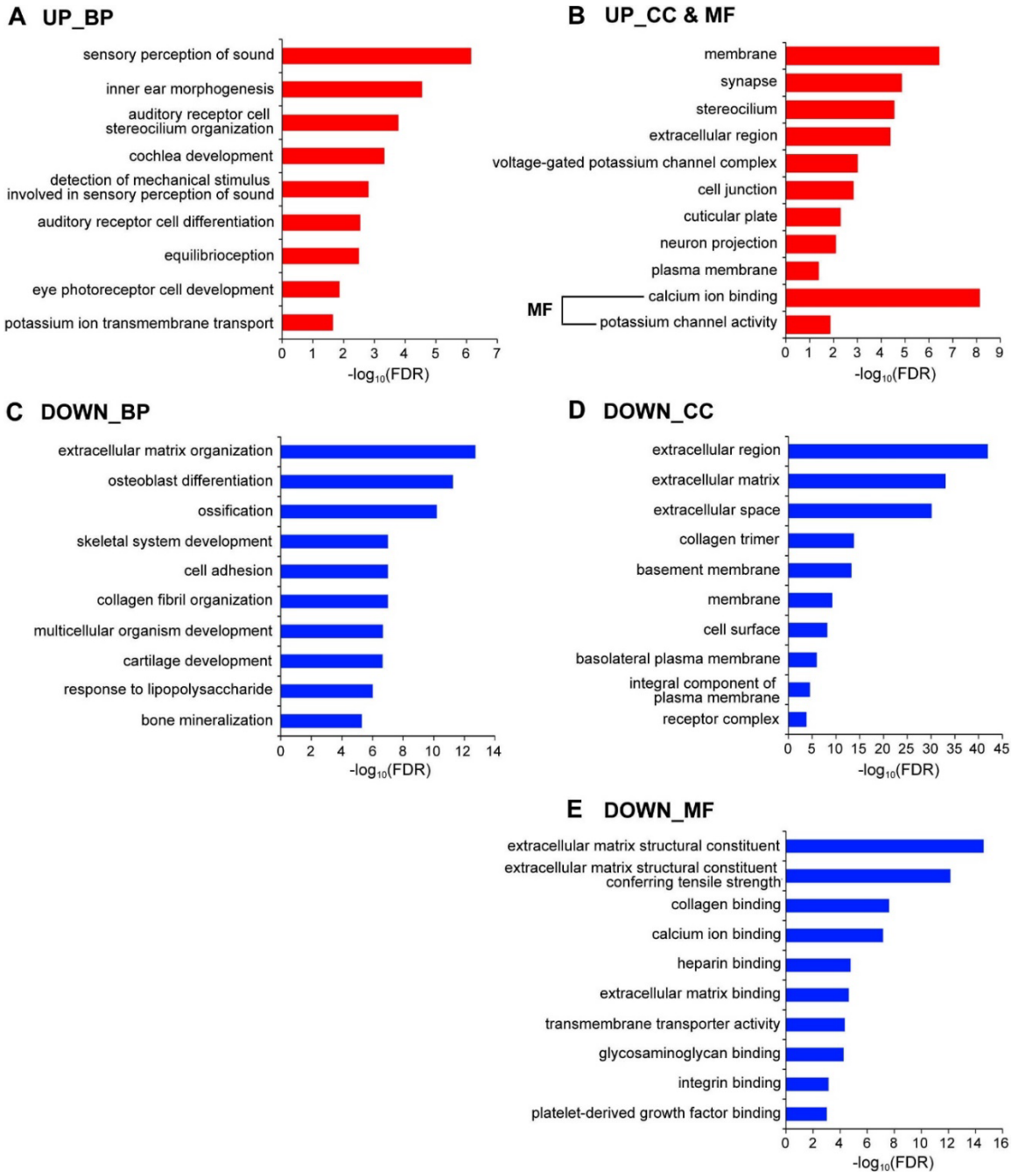

Fig. S13. GO terms enriched among genes with increasing (UP) or decreasing (DOWN) expression gradients along the cochlear duct. (**A-B**) All statistically significant GO terms for the UP group are shown. These included 9 terms for biological processes (BP), 9 terms for cellular components (CC), and 2 terms for molecular function (MF). (**C-E**) The top 10 GO terms in the BP, CC, and MF categories for the DOWN group. *P*-values for each GO term and the gene lists are provided in Table S3.

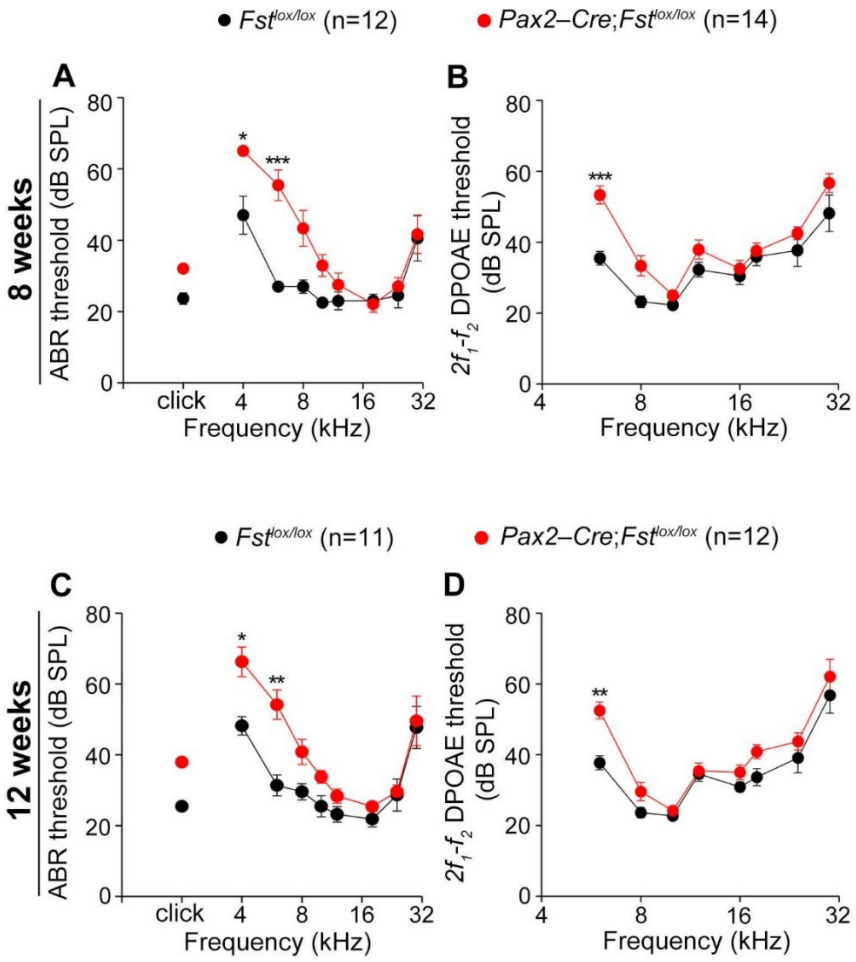

Fig. S14. Low-frequency hearing loss is maintained until at least 3 months of age in *Fst* cKO mutants. (**A–D**) ABR analyses in 8 and 12-week-old *Fst*$^{lox/lox}$ and *Pax2-Cre*; *Fst*$^{lox/lox}$ mice. ABR thresholds to click and individual frequencies in *Fst*$^{lox/lox}$ and *Pax2-Cre*; *Fst*$^{lox/lox}$ mice (**A, C**). $2f_1$-f_2 DPOAE thresholds in *Fst*$^{lox/lox}$ and *Pax2-Cre*; *Fst*$^{lox/lox}$ mice (**B, D**). Data are presented as means ± standard error. Statistical comparisons were determined via two-way ANOVA with Bonferroni corrections for multiple comparisons (n.s., non-significant, **P* < 0.05, ***P* < 0.01, and ****P* < 0.001).

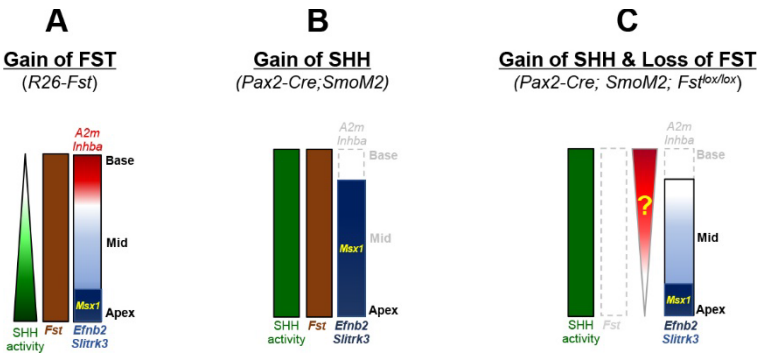

Fig. S15. Diagram illustrating changes in regional markers in FST or SHH mutant cochlea. While gain of FST function does not change regional identity (**A**), gain of SHH function induces apical identity at the expense of basal identity along the entire length of the cochlea (**B**). Gain of SHH function fails, however, to induce apical identity along the entire cochlea in the absence of FST (**C**). These results suggest strong SHH can only induce ectopic apical identity in the presence of FST. In addition, the restoration of the expression gradients for the apical markers *Msx1* and *Slitrk3* (**C**) suggests the presence of unknown graded signal(s), stronger at the base and weaker toward the apex, that inhibit the apical identity induced by SHH signaling.

Supplementary Tables.

Tables S1-S4 are provided as separate files in spreadsheet format

Table S1. List of genes in the UP and UP-1 groups

Table S2. List of genes in the DOWN and DOWN-1 groups

Table S3. Gene lists of GO terms in the UP and DOWN groups

Table S4. Upstream regulator analysis with IPA for the UP-1 and DOWN-1 groups

SI References

1. M. M. Matzuk *et al.*, Multiple defects and perinatal death in mice deficient in follistatin. *Nature* **374**, 360-363 (1995).
2. M. M. Matzuk *et al.*, Functional analysis of activins during mammalian development. *Nature* **374**, 354-356 (1995).
3. C. J. Jorgez, M. Klysik, S. P. Jamin, R. R. Behringer, M. M. Matzuk, Granulosa cell-specific inactivation of follistatin causes female fertility defects. *Mol Endocrinol* **18**, 953-967 (2004).
4. T. Ohyama, A. K. Groves, Generation of Pax2-Cre mice by modification of a Pax2 bacterial artificial chromosome. *Genesis* **38**, 195-199 (2004).
5. M. Prajapati-DiNubila, A. Benito-Gonzalez, E. J. Golden, S. Zhang, A. Doetzlhofer, A counter gradient of Activin A and follistatin instructs the timing of hair cell differentiation in the murine cochlea. *Elife* **8** (2019).
6. H. Morsli, D. Choo, A. Ryan, R. Johnson, D. K. Wu, Development of the mouse inner ear and origin of its sensory organs. *J Neurosci* **18**, 3327-3335 (1998).
7. H. Ankamreddy *et al.*, Region-specific endodermal signals direct neural crest cells to form the three middle ear ossicles. *Development* **146** (2019).
8. E. J. Son *et al.*, Developmental gene expression profiling along the tonotopic axis of the mouse cochlea. *PLoS One* **7**, e40735 (2012).
9. E. J. Son *et al.*, Conserved role of Sonic Hedgehog in tonotopic organization of the avian basilar papilla and mammalian cochlea. *Proc Natl Acad Sci U S A* **112**, 3746-3751 (2015).
10. K. H. Moon *et al.*, Dysregulation of sonic hedgehog signaling causes hearing loss in ciliopathy mouse models. *Elife* **9** (2020).
11. C. A. Schneider, W. S. Rasband, K. W. Eliceiri, NIH Image to ImageJ: 25 years of image analysis. *Nature methods* **9**, 671-675 (2012).
12. W. Han *et al.*, Distinct roles of stereociliary links in the nonlinear sound processing and noise resistance of cochlear outer hair cells. *Proc Natl Acad Sci U S A* **117**, 11109-11117 (2020).
13. D. W. Huang, B. T. Sherman, R. A. Lempicki, Systematic and integrative analysis of large gene lists using DAVID bioinformatics resources. *Nature protocols* **4**, 44-57 (2009).